Journal of Electronic Materials (2023) 52:2336–2346
https://doi.org/10.1007/s11664-022-10162-3

ORIGINAL RESEARCH ARTICLE

N-Doped Graphene-Supported Gold Nanorods for Electrochemical Sensing of Ascorbic Acid with Superior Sensitivity

Shiyi Yang[1] · Yudan Cheng[1] · Deyi Cheng[1] · Yifeng Wang[1] · Hui Xu[1,4] · Mei Li[2] · Tingting Jiang[3] · Hua Wang[4,5]

Received: 21 April 2022 / Accepted: 9 December 2022 / Published online: 16 January 2023

Abstract

Gold nanorod (AuNR)-decorated N-doped graphene (NG) was designed for the electrocatalytic detection of ascorbic acid (AA). The synergistic effect of NG with higher surface area, large number of binding sites for AuNRs, good conductivity and electrocatalytic activity, and AuNRs with higher surface area, faster electron-transfer ability, and special electrocatalytic performance achieves superior sensitivity for monitoring of AA. All kinds of spectral and morphological test methods were applied to characterize the prepared NG and AuNRs. Under the optimized pH, two wide linear relationships between the peak current and the AA concentration by differential pulse voltammetry (DPV) within the ranges of 5×10^{-9} M to 1×10^{-6} M, and 1×10^{-6} M to 8×10^{-3} M were observed, with a detection limit as low as 2.6 nM. In addition, high reproducibility, stability, and great potential in the quantification of AA in diluted real human serum were also achieved by the combined electrochemical sensor. All the results indicate that the AuNR/NG sensing interface can be used as a promising material in the field of electrochemical sensors.

Graphical Abstract

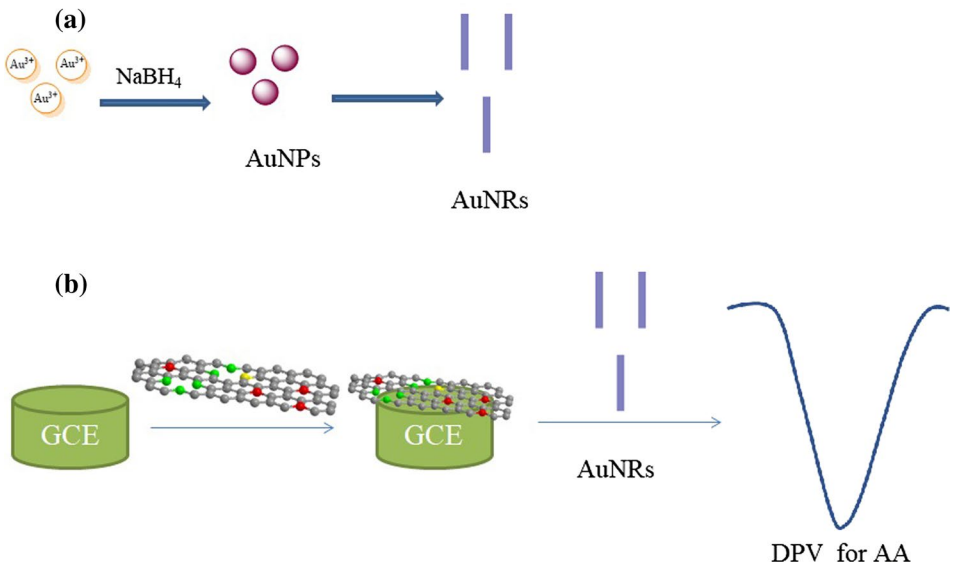

Keywords Gold nanorods · N-doped graphene · ascorbic acid · electrocatalytic detection

Shiyi Yangand Yudan Cheng contributed equally to this work.

Extended author information available on the last page of the article

Introduction

After the discovery of graphene in 2004,[1] the real, wide exploration of two-dimensional nanomaterials began. Graphene is an exciting single-atom-thick sheet of sp^2-bonded carbon that is packed in a hexagonal honeycomb lattice.[2–4] Currently, N-doped graphene (NG) is appealing because the different dopant configurations of N (graphitic N, pyridinic N, pyrrolic N, nitrilic N, and oxidized N) can affect the local charge distribution, resulting in different electronic, catalytic, and sensing properties.[5] Theoretical and experimental studies both revealed that doping graphene with nitrogen is an effective way to modulate its electronic arrangement and chemical reactivity.[6–8] C is substituted via N and a single pair of electrons, affecting sp^2 carbon atoms[9] and enhancing the conductivity and electrocatalytic activity.[10,11] Chemical vapor deposition (CVD),[12] plasma treatment,[13] thermal annealing,[14] and the hydrothermal method[15] are the main approaches for producing NG. Currently, the hydrothermal method is popular due to its simple operation. Ammonia,[16] pyridine,[17] acetonitrile,[18] and urea[19] are often used as nitrogen sources. When urea is used as the N precursor, it possesses good reduction capacity,[20] and high nitrogen content is often obtained.[21] At the same time, it has low toxicity and thus is beneficial for environmental protection.[22] With these advantages, urea is an ideal N precursor for preparing NG.

Metal nanoparticle-decorated NG[23,24] has been widely used in electrocatalytic applications. Among these materials, gold nanoparticles are promising due to their unique properties.[25,26] The past two decades have witnessed the rapid development of gold nanostructure-based electrochemical sensing owing to their excellent electronic and catalytic performances. The nanoparticle geometry significantly affects their physical and chemical properties. Compared with spherical nanoparticles, nonspherical gold nanocrystals demonstrate an anisotropic optical and electronic response. Gold nanorods (AuNRs) have received considerable attention due to their higher surface area, faster electron-transfer ability, and good biocompatibility, thus improving the sensitivity and selectivity of the electrochemical sensors.[27–30] In addition, the rod length can be adjusted by varying the AA concentration.[31] AuNR-coated graphene,[32] graphene oxide sheets, [33] and reduced graphene oxide[34] have been reported for the electrochemical detection of hydrogen peroxide, DNA and dihydro-nicotinamide adenine dinucleotide (NADH), respectively. However, to our knowledge, there are no reports about AuNR-decorated NG-based electrocatalysis for detecting small molecules.

Herein, NG synthesized by hydrothermal method from graphite oxide and urea was integrated with AuNRs for monitoring ascorbic acid (AA). NG provides a higher surface area, a large number of binding sites for AuNRs, good conductivity, and electrocatalytic activity, while AuNRs possess higher surface area, faster electron-transfer ability, and special electrocatalytic performance. The synergistic effect of the three-dimensional AuNR/NG/GCE-sensing interface improves the catalytic performance, increasing its response signal for AA monitoring. The successful construction of this sensor indicates that the combination of NG and AuNRs is promising for the development of electrochemical sensors.

Experimental

Chemicals

Chloroauric acid hydrate ($HAuCl_4 \cdot 4H_2O$) and D-(+)-glucose (Glu) anhydrous were obtained from Sinopharm Chemical Reagent Co., Ltd. L-Ascorbic acid (L-AA, > 99.7%) was obtained from Tianjin Ruijinte Special Chemicals Reagent Co., Ltd. Dopamine hydrochloride (DA·HCl), L-glutathione reduced (L-GSH, > 98.0%), and hexadecyltrimethylammonium bromide (CTAB, > 99.0%) were purchased from Sigma-Aldrich. All other chemicals were analytical grade and used directly without additional purification. All the solutions were prepared using ultrapure water (conductivity of 18.25 MΩ·cm).

Apparatus and Instruments

All the electrochemical measurements were recorded in a CHI-660C electrochemical workstation (CH Instruments, Shanghai, China) with a conventional three-electrode system, which consists of an Ag/AgCl (3.0 M KCl) electrode as a reference electrode, a Pt wire as auxiliary electrode, and a modified glass carbon electrode (GCE, 3 mm in diameter) as working electrode. High-resolution field emission scanning electron microscopy (FESEM; SU-8010, Hitachi, Japan) and transmission electron microscopy (TEM, JEM-1230, JEOL) at an accelerating voltage of 100 kV were used to characterize the morphology of the prepared AuNRs and NG. A UV-2550 spectrometer (Shimadzu, Japan) was used to obtain the absorption spectra of the AuNRs. Raman spectra were acquired using a Horiba spectrometer (LabRAM HR Evolution, Japan) set to an excitation wavelength of 532 nm.

Preparation of NG and AuNRs

First, graphene oxide (GO) was produced following the modified Hummers method.[35] NG was prepared with appropriate modification from GO and urea via a simultaneous GO hydrothermal reduction and N doping process.[36] Three milliliters 0.5 g/L of GO dispersion was mixed with

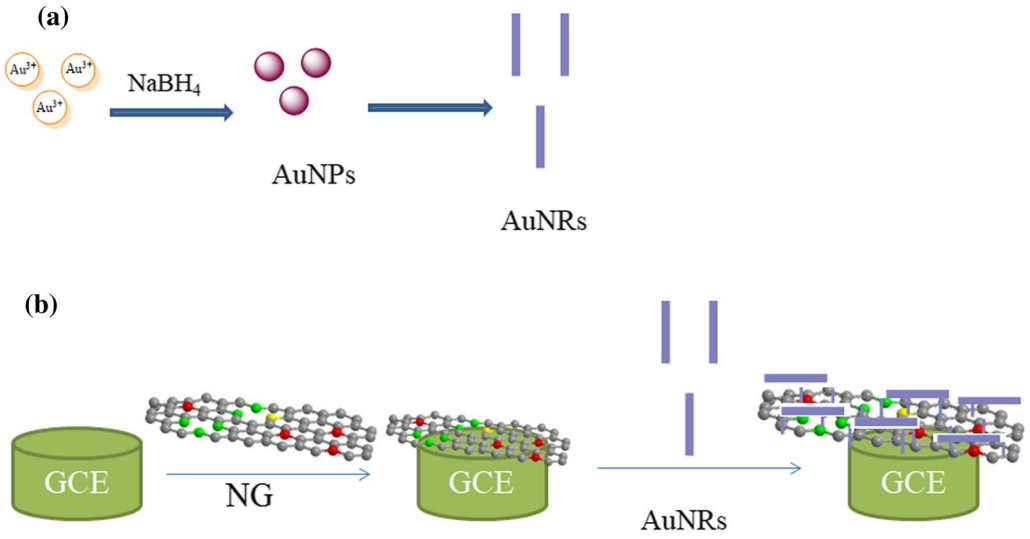

Scheme 1. The schematic process for electrode preparation.

27 mL deionized water to obtain 30 mL GO dispersion. Then, 0.45 g urea was added to the solution and stirred for 30 min (GO: urea = 1:300). Finally, the mixture was sealed in a 50 mL Teflon-lined stainless reactor and maintained at 160°C for 3 h. After centrifugation and washing with water several times, the collected sample was freeze-dried.

AuNRs were prepared by the seeded growth method with moderate modification[31,37] as follows. The first step is the reduction of $HAuCl_4 \cdot 4H_2O$ (5×10^{-4} mol/L, 5 mL) by freshly prepared, ice-cold $NaBH_4$ (0.6 mL 0.01 M) to prepare gold seed nanoparticles in the presence of 0.075 M CTAB (0.2 mol/L 2.5 mL). The obtained solution was stirred vigorously for 2 min. After 24 h at 25°C in a water bath, the solution became a brown color and the seed nanoparticles were formed.

The second step is the preparation of AuNRs. Five milliliters 0.2 mol L^{-1} CTAB aqueous solution was added to 0.6 mL 4 mM $AgNO_3$ solution at 30°C (the use of $AgNO_3$ can improve the yield of AuNRs and obtain controlled aspect ratios). After the addition of 5 mL of 0.01 M chloric acid solution, the solution was stirred slowly until it turned yellow. Then, 700 µL 0.1 M AA solution was added and the solution became colorless. Finally, 12 µL gold seed prepared in the first step was added and the solution was stirred vigorously for 2 min. Bluish-violet AuNRs were obtained after the solution was maintained at 28°C for an additional 18 h. Finally, excess CTAB was removed by centrifugation of the solution at 25°C and 12,000 rpm for 10 min, after which the AuNRs were re-dispersed in water.

Construction of the Sensors

A simple dipping approach was used to fabricate the electrodes. First, the GCE was polished using Al_2O_3 powder with size of 1.0 µm, 0.3 µm, and 0.05 µm, respectively, and then ultrasonicated in ethanol and deionized water for 1.0 min in succession. A mixture of 1.0 mg/mL NG aqueous solution was ultrasonically dispersed for 3 h to obtain NG suspension. Five microliters of the prepared NG suspension was dropped directly onto the surface of the drying GCE followed by drying at 50°C. Then 5 µL of AuNRs solution was directly added to the surface of the NG and dried at 80°C to obtain homogeneous and adequate coverage. For the detection of AA, the bare GCE or the modified electrode was used as the working electrode in 0.1 M PBS (pH 7.4) containing different concentrations of AA or other small molecules (DA, GSH, and Glu). The schematic process of electrode preparation is displayed in Scheme 1.

Results and Discussion

Characterization of NG and AuNRs

The morphology of the prepared NG and AuNRs was observed by SEM and TEM. As shown in Fig. 1, SEM images (Fig. 1a) of NG demonstrated a film-like structure with many ripples. The unique large stacked nanosheets were confirmed by TEM images (Fig. 1c). Figure 1b shows the EDX spectrum of NG, and C, N, and O atoms were detected in the NG. The atomic percentage of N in particular was as high as 16.56%. The obvious sheet structure of

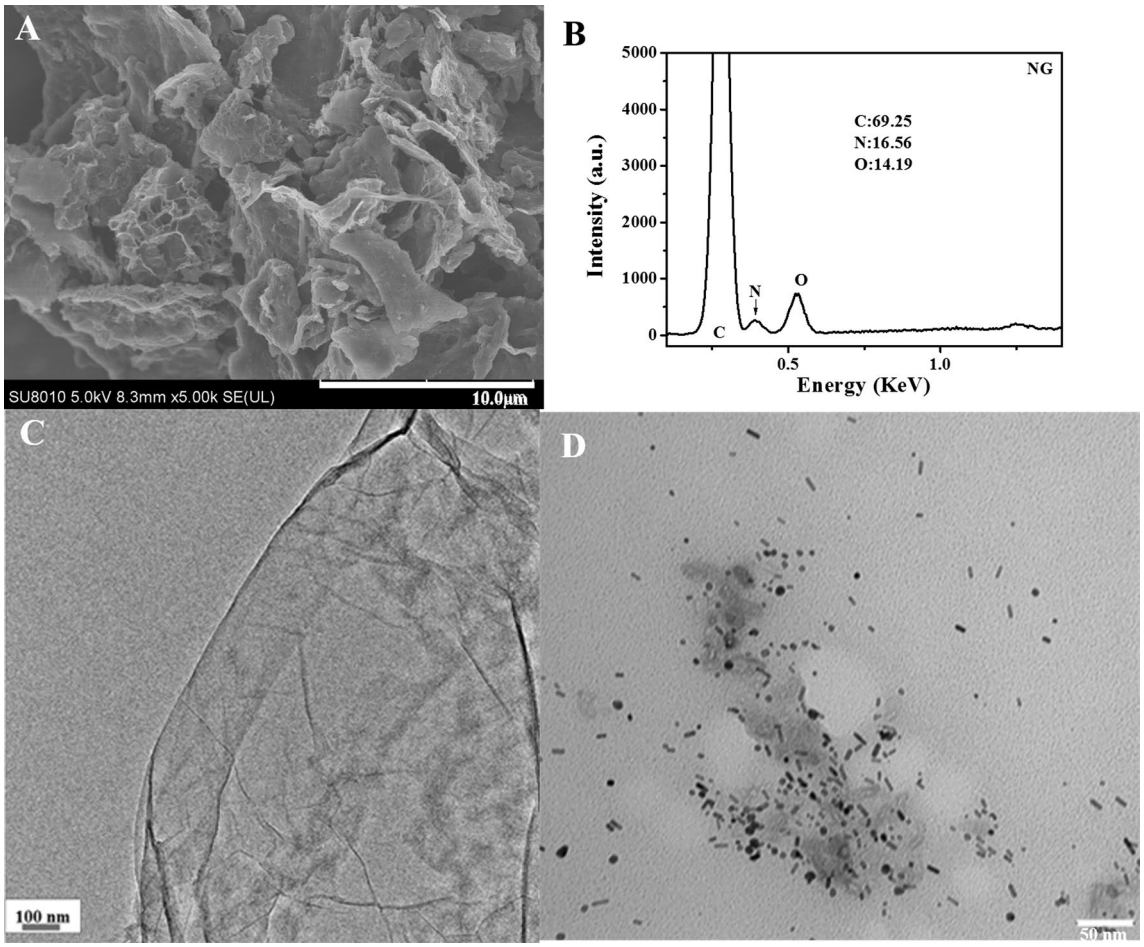

Fig. 1 SEM images of NG (a), EDX spectrum of NG (b), TEM images of NG (c) and AuNR/NG mixture (d).

NG demonstrated that NG possessed a large surface area for adhering of AuNRs (Fig. 1d). Rodlike AuNRs were distributed evenly on the surface of NG, resulting in the successful assembly of the AuNR/NG mixture.

Then, x-ray photoelectron spectroscopy (XPS) survey was used to estimate the chemical composition and N-doping configuration of NG. Three peaks of C 1*s* (284.8 eV), O 1*s* (532.7 eV), and N 1*s* (399.3 eV) were observed (Fig. 2a). The C 1*s* peak in the NG can be deconvoluted into three peaks (Fig. 2b), namely, C–C (283.8 eV), C–N (285.4 eV), and C–O functional groups (288.5 eV),[38] respectively. Three peaks appearing in the O 1*s* spectrum at 531.3 eV, 532.2 eV, and 533.4 eV (Fig. 2c) were attributed to C=O, C–O, and O=C–O.[24] The N 1*s* spectrum of NG reveals that up to 13.92 at.% N was a combination of pyridinic N (398.8 eV), amino N (399.1 eV), and pyrrolic N (399.6 eV)[39,40] (Fig. 2d). These results indicate that N was successfully doped into NG. At the same time, the pyridinic N is particularly useful for improving the electrochemical performance of carbon materials,[41,42] while pyrrolic N can maintain the graphitic phase structure of sp^2 hybridization and enhance electrical conductivity by providing delocalized electrons.[43]

It is well known that AuNRs are an outstanding sensing material due to their superior electrical conductivity and signal amplification performance. AuNRs were synthesized by seed-mediated synthesis.[31,37] First, ultraviolet–visible (UV–Vis) spectra were used to confirm the formation of AuNRs. As demonstrated in Fig. 3a, an absorption peak centered at 526 nm appeared when gold seed nanoparticles were formed by reduction of $HAuCl_4$ by $NaBH_4$ and demonstrated the characteristic surface plasmon resonance absorption of seed nanoparticles. Then, the seed was added to a growth solution containing CTAB, $AgNO_3$, $HAuCl_4$, and AA. A new plasmon band at 742.30 nm appeared, demonstrating the formation of AuNRs (Fig. 3b). It can be seen from the TEM images that most of the AuNRs with length of about 20 nm and width of about 10 nm were dispersed in the obtained solution (Fig. 3c), demonstrating an aspect ratio of about 2.0 ± 0.4 (calculated from 280 AuNRs), with a small number of spherical nanoparticles (Fig. 3c). In addition, the intensity ratios of G mode (1586.5 cm^{-1}, Raman-allowed

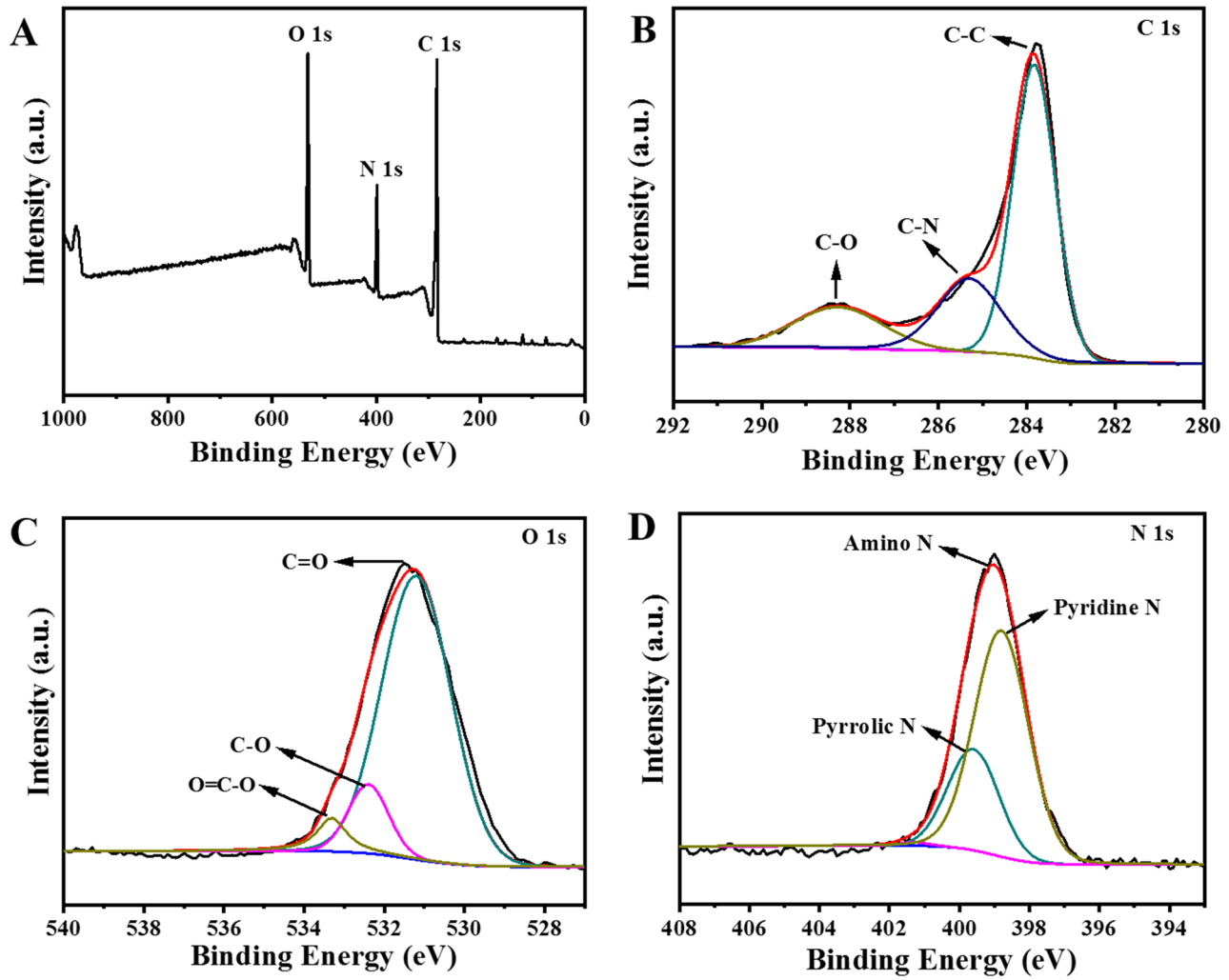

Fig. 2 XPS spectra of NG (a), XPS C 1*s* spectrum (b), XPS O 1*s* spectrum (c), and XPS N 1*s* spectrum (d).

phonon high-frequency mode) and D mode (1326.3 cm^{-1}, disordered-induced peak) change for GO, NG, and AuNR/NG are 0.88, 0.92 and 0.97, respectively. I_G/I_D increases due to the transformation from GO with many oxygenated functional groups to NG and modification of AuNRs, confirming the formation of N-doping and AuNR loading.

Electrochemical Properties of AuNR/NG/GCE

The electrochemical properties of GCE, NG/GCE, and AuNR/NG/GCE were first studied via electrochemical impedance spectroscopy (EIS) because it can explore the interface between the electrode and electrolyte. The diameter of the semicircle in the EIS curve represents the resistance in electron transfer kinetics, the resistance charge transfer (Rct), which controls the electron-transfer kinetics of the redox probe at the electrode–electrolyte interface. Using 5 mM $Fe(CN)_6^{3-/4-}$ in 0.1 M KCl as redox probe to examine the interface characteristics, the diameters of the semicircle of the modified electrodes are much smaller (almost disappearing) than that of the undecorated electrode (Fig. 4a), verifying the good conductivity of NG/GCE and AuNR/NG/GCE.

Then, cyclic voltammetry (CV) from −0.40 to 0.60 V with 1 mM AA in 0.1 mol L^{-1} PBS (pH = 7.4) is used to investigate the electrocatalytic property of various modified electrodes. It can be seen from Fig. 4b that an oxidation process appeared during the anodic scanning in all cases without a reduction process during the cathodic scanning, suggesting an irreversible oxidation reaction of AA. The bare GCE only had a weak response current at a higher potential (about 0.36 V) for AA monitoring. The peak current acquired on the NG-modified electrode was higher than that of the bare GCE, and the oxidation potential exhibited a considerable negative shift, showing good electron transfer capacity and conductivity. Furthermore,

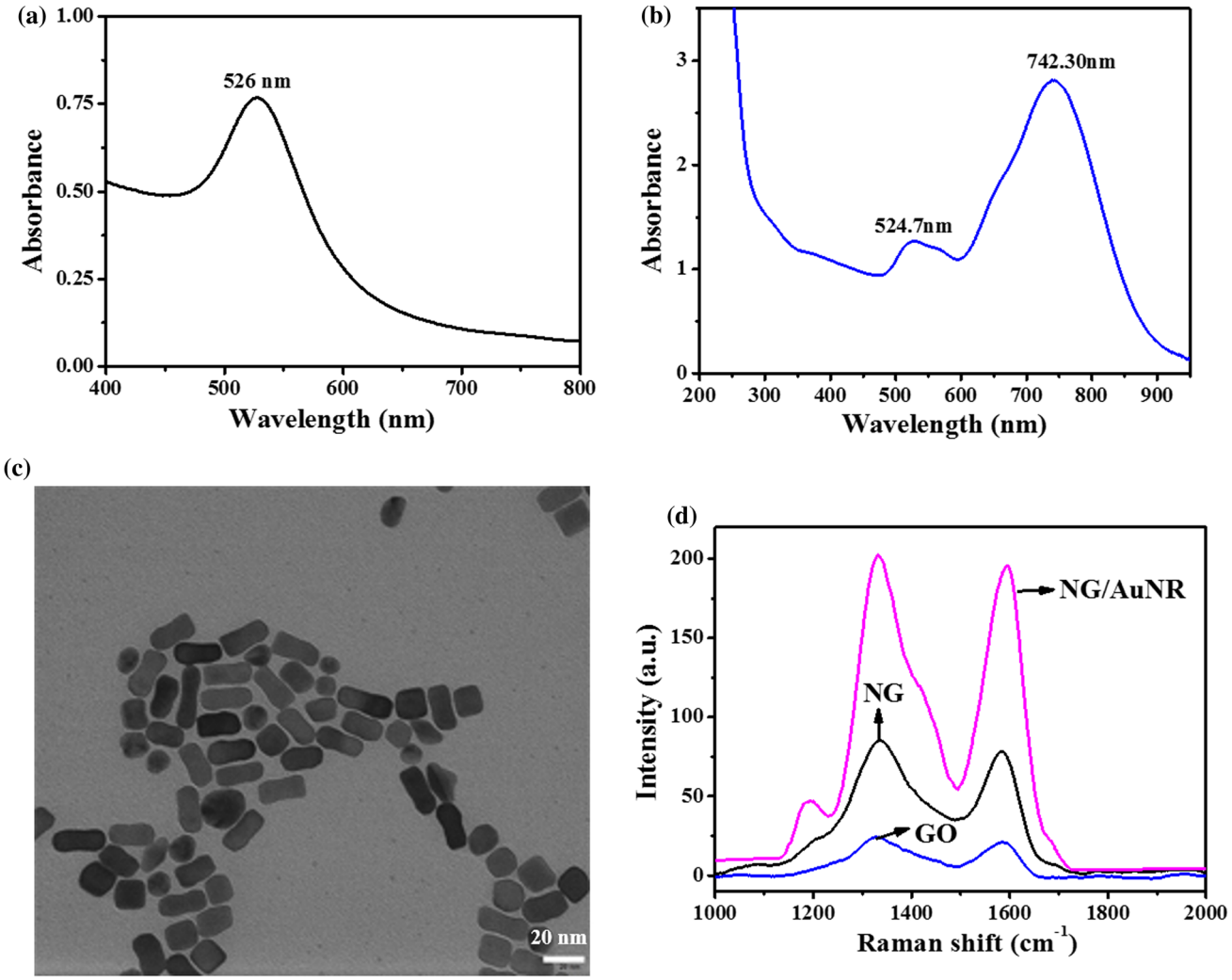

Fig. 3 UV–Vis spectra of gold nanoparticles (a), AuNRs (b), TEM images of prepared AuNRs (c), and Raman spectra of GO, NG, and NG/AuNR (d).

the AuNR/NG-modified electrode produced the highest current and the most negative potential compared to other electrodes. It is worth noting that the oxidation potential value is below 0.03 V, indicating a very low potential on the surface of AuNR/NG/GCE for the electro-oxidation of AA via CVs. The 1-D nanostructure of the AuNRs possesses general properties similar to gold nanoparticles. In addition, they possess some superior advantages over spherical gold nanoparticles, such as higher surface area, faster electron-transfer ability, and special electrocatalytic performance.[28,29] The synergistic effect of NG and AuNRs enabled electrochemical detection with promising results.

Effect of pH and Scan Rate

The influence of pH value on the performance of AA sensing was investigated. The effect of electrolyte pH from 6.0 to 8.5 on AA electro-oxidation on AuNR/NG/GCE was studied, as shown in Fig. 5a. The oxidation peak current and the potential changed with the change in electrolyte pH. The highest amperometric response was pH 7.4 (Fig. 5b), and the most negative oxidation potential (E_p) was also at pH 7.4 (Fig. 5b). It is worth noting that the pH of human blood is approximate 7.4, so optimum pH of 7.4 was chosen in our following experiments.

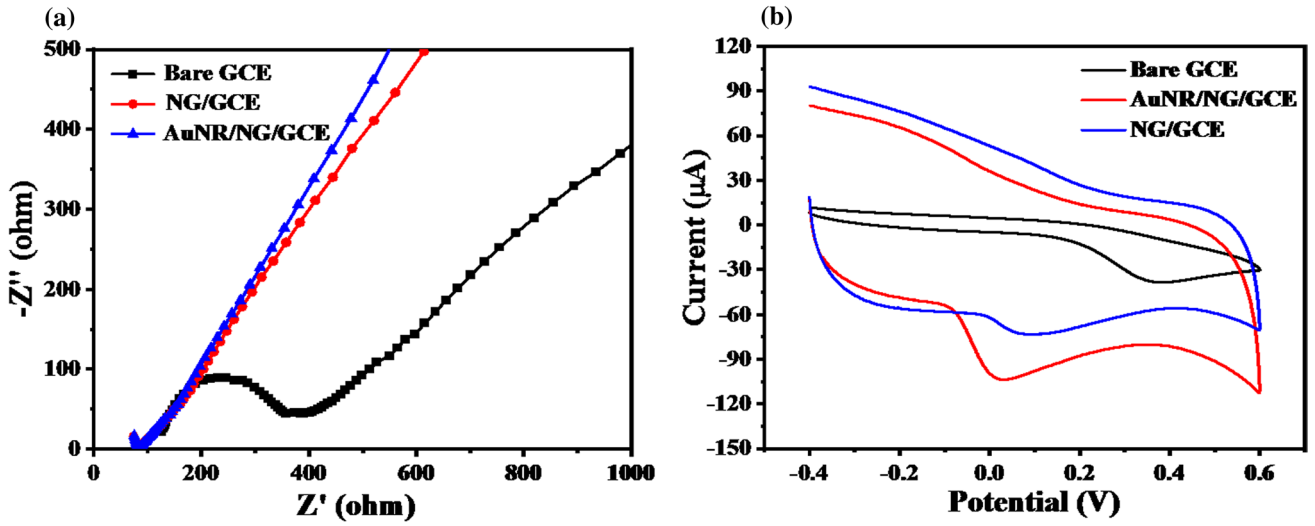

Fig. 4 (a) EIS plots performed in 5 mM $K_3Fe(CN)_6$ and $K_4Fe(CN)_6$ containing 0.1 M KCl for bare GCE, NG/GCE, and AuNR/NG/GCE; (b) CVs of (a) bare GCE, NG/GCE, and AuNR/NG/GCE containing 1 mM AA in 0.1 M PBS (pH = 7.4) at a scan rate of 0.1 V/s.

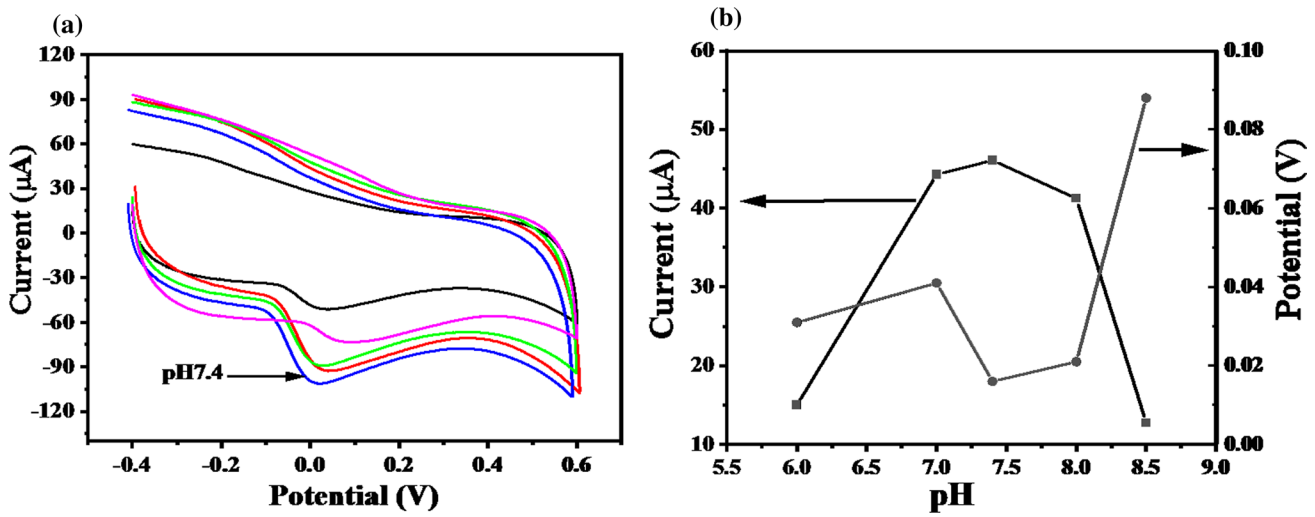

Fig. 5 (a) AuNR/NG/GCE with 1 mM AA under different pH levels at a scan rate 0.1 V/s in 0.1 M PBS (black line: pH 6.0, red line: pH 7.0, blue line: pH 7.4, green line: pH 8.0, pink line: pH 8.5). (b) The corresponding plot of pH versus I_{pa} and pH vs E_p (Color figure online).

The Effect of Scan Rate

To investigate the electrode reaction process, the effect of scan rate on the electrooxidation of AA was explored in 0.1 M PBS (pH 7.4) containing 1 mM AA at various scan rates (50–300 mV/s). As demonstrated in Fig. 6a, the oxidation peak currents increased linearly when the scan rate increased. Their relationship can be described by the linear equation: I_p (μA) = 0.080 V (mV/s) + 37.578 (R = 0.999) (Fig. 6 b). The result indicated that the peak current is proportional to the scanning speed and the electrochemical oxidation of AA at the AuNR/NG/GCE sensing interface is mainly controlled by the adsorption process. The oxidation potentials increased slightly with the increase of the scan rate, and a linear relationship of Epa versus ln v for AA is presented in Fig. 6c (E_{pa} = 0.0337lnυ-0.121; r = 0.997). According to Laviron's theory and the following equation $E_{pa} = E^0 + \frac{RT}{(1-\alpha)nF}\ln v$, where α is the charge transfer coefficient and n is the number of electrons transferred. Therefore, n can be calculated for electro-oxidation of AA at AuNR/NG/GCE from the slope of E_p versus ln v as 1.5 (approximately 2), suggesting that the electrode process of AA at the AuNR/NG/GCE is not completely irreversible one, which is consistent with the CV of AA at Figs. 4b and 6a.

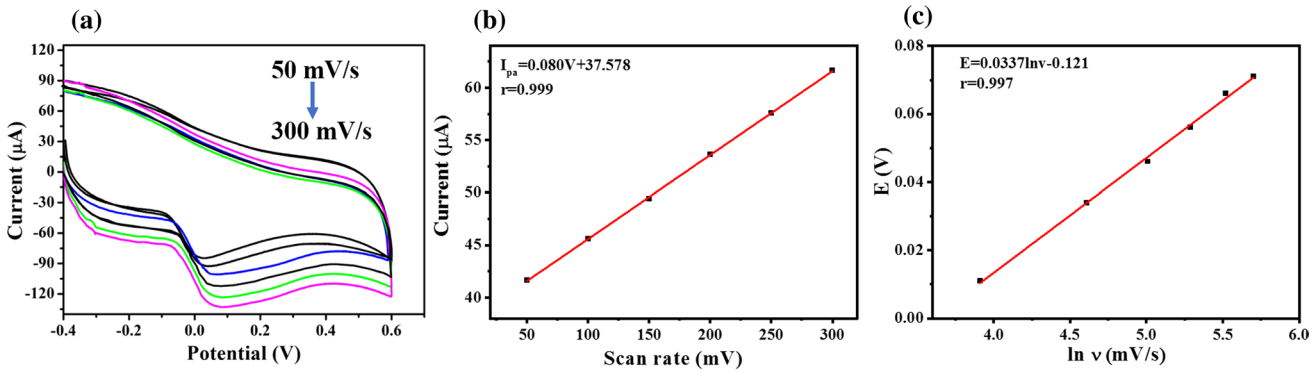

Fig. 6 (a) CVs of AuNR/NG/GCE in 0.1 M PBS (pH 7.4) containing 1 mM AA at a scan rate of 50–300 mV/s. (b) Calibration plot of I_{pa} versus the scan rate. (c) The linear relationship of the oxidation peak potential and ln *v*.

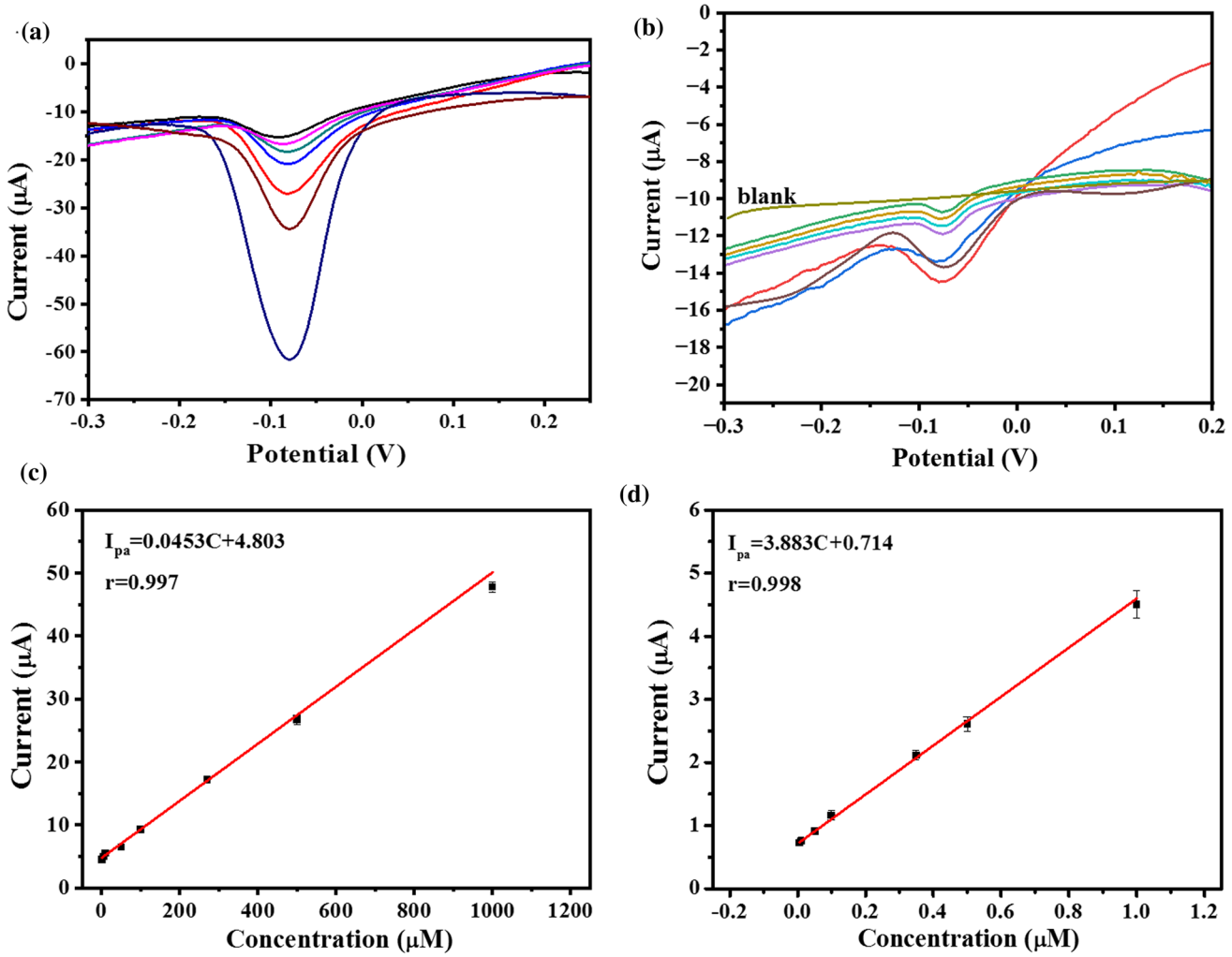

Fig. 7 (a) DPV curves of NG/AuNRs modified electrode in 0.1 M PBS (pH = 7.4) containing different concentrations of AA from 1×10^{-6}–1×10^{-3} M and (b) the concentration of AA from 5×10^{-9}–1×10^{-6} M. (c) and (d) Linear relationships of different concentration ranges.

Determination of AA using AuNR/NG Modified GCE

Differential pulse voltammetry (DPV) analysis of the AuNR/NG/GCE was performed with different AA concentrations in phosphate buffer. As Fig. 7a and c show, the oxidation peak currents increase gradually when the concentration of AA increased. The oxidation peak current correlates linearly with the AA concentration in a wide range from 1×10^{-6} to 1×10^{-3} M and 5×10^{-9} to 1×10^{-6} M, with perfect correlation coefficients of 0.997 and 0.998 (Fig. 7b and d). The blank in the absence of AA shows almost no obvious oxidation peak, demonstrating no interference from the addition of AA during the synthesis of AuNRs. As AA is easily oxidizable, we think it is also the case in the adsorbed state after the adsorbed AuNRs were dried at 80°C (Fig. 7). The detection limit can be calculated to be 2.6 nM ($S/N=3$) based on the linear range 5×10^{-9} to 1×10^{-6} M, which is lower than most reported references.[44–52] Last but not least, the two wide linear ranges are interesting and may show promise for further application.

Selectivity, Stability, and Reproducibility of the Sensor

In addition to high sensitivity, selectivity and stability are crucial parameters in electrochemical sensing applications. The selectivity of AuNR/NG/GCE towards AA monitoring was evaluated in the presence of common electroactive interfering substances including DA, GSH, and Glu. The results in Fig. 8 show that the oxidation current of AA was not significantly affected by these interfering substances, with an acceptable error smaller than 6%. The long-term stability was analyzed by detecting 5 μM AA for 20 days under optimized conditions, where 89.9% of the peak current was maintained after 15 days, showing acceptable stability of the sensing systems.

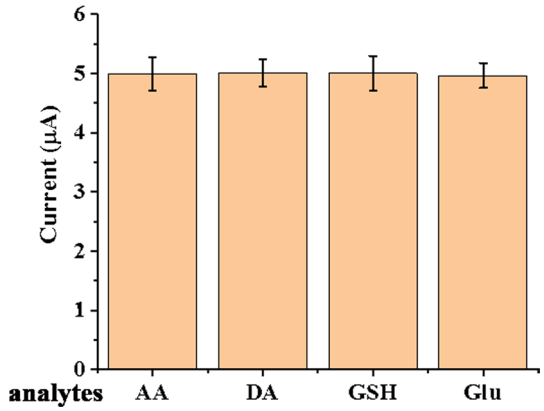

Fig. 8 DPV current response of the different species of small biomolecules with 5 μM AA, and the concentration of other analytes (DA, GSH, or Glu) is 1 μM. Error bars show the standard deviation of measurements via three independent surveys.

Table I Results using the modified electrode from analysis of AA in diluted human serum

Sample used	Added (μM)	Found (μM)	Recovery (%)	RSD (%) ($n=3$)
Serum	80	77.9	97.38	0.99
	0.05	0.04895	97.9	1.27
	0.008	0.0088	110.0	3.08

The reproducibility of the electrochemical AA sensor was then investigated. Five different AuNR/NG/GCEs were independently fabricated and were used to detect 5 μM and 5×10^{-4} M AA, respectively. The relative standard deviation (RSD) obtained for five measurements was 4.5% (5 μM AA) and 3.2% (5×10^{-4} M AA), indicating the excellent reproducibility of the sensing platform.

Real Sample Application

By adding 80 μM, 0.05 μM, or 0.008 μM of standard AA solution to a given diluted human serum sample (100 μL was diluted to 10 mL using 0.1 M PBS, pH 7.4), the electrochemical sensor was applied to evaluate its practical applicability by the standard addition method. DPV of 80 μMAA showed no obvious change after adding diluted human serum (Fig. S1 in Supporting Information), indicating no effect from the sample matrix. Using the modified electrode, analysis results demonstrated in Table I revealed excellent recovery percentages from 97.38% to 110.0% ($n=3$). The above results indicate that significant matrix interference was avoided using the modified electrode.

Conclusion

AuNRs immobilized on NG-modified GCE was used as an electrochemical sensor for the determination of AA. Different from GO and graphene, NG has better conductivity than GO and more active sites than graphene, resulting in improved electrocatalytic activity. Compared with GCE, a significant increase in oxidation current signal and decrease in the overpotential for AA oxidation was achieved, which originated from the synergistic effect of NG and AuNRs: higher surface area, faster electron-transfer ability, good conductivity, and excellent electrocatalytic activity. A very low detection limit of 2.6 nM was obtained using the modified electrode. Under the applied conditions, AuNR/NG/GCE exhibited very good repeatability and stability. In addition, this electrode showed potential for the determination of AA in diluted human serum.

Supplementary Information The online version contains supplementary material available at https://doi.org/10.1007/s11664-022-10162-3.

Acknowledgments This work was supported by the Natural Science Foundation of Shandong Province, China (ZR2020MB075, ZR2020MC079) and the national innovation and entrepreneurship training program for college students (202113287103).

Conflict of interest The authors declare that they have no conflict of interest.

References

1. K.S. Novoselov, A.K. Geim, S.V. Morozov, D. Jiang, Y. Zhang, S.V. Dubonos, I.V. Grigorieva, and A.A. Firsov, Electric field effect in atomically thin carbon films. *Science* 306, 666 (2004).
2. A.K. Geim and K.S. Novoselov, The rise of graphene. *Nat. Mater.* 6, 183 (2007).
3. D. Li and R.B. Kaner, Graphene-based materials. *Science* 320, 1170 (2008).
4. M.J. Allen, V.C. Tung, and R.B. Kaner, Honeycomb carbon: a review of graphene. *Chem. Rev.* 110, 132 (2010).
5. T. He, A.R.P. Santiago, and A. Du, Atomically embedded asymmetrical dual-metal dimers on N-doped graphene for ultra-efficient nitrogen reduction reaction. *J. Catal.* 388, 77 (2020).
6. M. Deifallah, P.F. McMillan, and F. Corà, Electronic and structural properties of two-dimensional carbon nitride graphenes. *J. Phys. Chem. C* 112, 5447 (2008).
7. Y. Li, Z. Zhou, P. Shen, and Z. Chen, Spin gapless semiconductor−metal−half-metal properties in nitrogen-doped zigzag graphene nanoribbons. *ACS Nano* 3, 1952 (2009).
8. M. Skorupska, A. Ilnicka, and J.P. Lukaszewicz, The effect of nitrogen species on the catalytic properties of N-doped graphene. *Sci. Rep.* 11, 23970 (2021).
9. D. Deng, X. Pan, L. Yu, Y. Cui, Y. Jiang, J. Qi, W.X. Li, Q. Fu, X. Ma, and Q. Xue, Toward N-doped graphene via solvothermal synthesis. *Chem. Mater.* 23, 1188 (2011).
10. Z. Mou, Y. Wu, J. Sun, P. Yang, Y. Du, and C. Lu, TiO_2 nanoparticles-functionalized n-doped graphene with superior interfacial contact and enhanced charge separation for photocatalytic hydrogen generation. *ACS Appl. Mater. Interfaces* 6, 13798 (2014).
11. L.S. Zhang, X.Q. Liang, W.G. Song, and Z.Y. Wu, Identification of the nitrogen species on N-doped graphene layers and Pt/NG composite catalyst for direct methanol fuel cell. *Phys. Chem. Chem. Phys.* 12, 12055 (2010).
12. Z. Zhai, H. Shen, J. Chen, X. Li, and Y. Jiang, Direct growth of nitrogen-doped graphene films on glass by plasma-assisted hot filament CVD for enhanced electricity generation. *J. Mater. Chem. A* 7, 12038 (2019).
13. S. Hu, F. Li, and Z. Fan, The comparison of property and visible light activity between bulk and surface doped N-TiO_2 prepared by sol–gel and N_2-plasma treatment. *Bull. Korean. Chem. Soc.* 33, 199 (2012).
14. M. Li, Z.S. Wu, W.C. Ren, H.M. Cheng, N.J. Tang, W.B. Wu, W. Zhong, and Y.W. Du, The doping of reduced graphene oxide with nitrogen and its effect on the quenching of the material's photoluminescence. *Carbon* 50, 5286 (2012).
15. Z.S. Wu, S.B. Yang, Y. Sun, K. Parvez, X.L. Feng, and K. Mullen, 3D nitrogen-doped graphene aerogel–supported Fe_3O_4 nanoparticles as efficient eletrocatalysts for the oxygen reduction reaction. *J. Am. Chem. Soc.* 134, 9082 (2012).
16. G. Singh, D.S. Sutar, B.V. Divakar, P.K. Narayanam, S.S. Talwar, R.S. Srinivasa, and S.S. Major, Study of simultaneous reduction and nitrogen doping of graphene oxide Langmuir–Blodgett monolayer sheets by ammonia plasma treatment. *Nanotechnology* 24, 355704 (2013).
17. G. Kim, S.H. Jhi, and N. Park, Effective metal dispersion in pyridinelike nitrogen doped graphenes for hydrogen storage. *Appl. Phys. Lett.* 92, 353 (2008).
18. T. Cui, R. Lv, Z.H. Huang, H. Zhu, F. Kang, K. Wang, and D. Wu, Effect of feed rate on the production of nitrogen-doped graphene from liquid acetonitrile. *Carbon* 50, 3659 (2012).
19. Z. Lin, G. Waller, Y. Liu, M. Liu, and C.P. Wong, Facile Synthesis of nitrogen-doped graphene via pyrolysis of graphene oxide and urea, and its electrocatalytic activity toward the oxygen-reduction reaction. *Adv. Energy Mater.* 2, 884 (2012).
20. J. Chen, Z. Mao, L. Zhang, Y. Tang, D. Wang, L. Bie, and B.D. Fahlman, Direct production of nitrogen-doped porous carbon from urea via magnesiothermic reduction. *Carbon* 130, 41 (2018).
21. N.B. Kristensen, A.C. Storm, and M. Larsen, Effect of dietary nitrogen content and intravenous urea infusion on ruminal and portal-drained visceral extraction of arterial urea in lactating Holstein cows. *J. Dairy Sci.* 93, 2670 (2010).
22. A. Seacat, P. Thomford, K. Hansen, G. Olsen, M. Case, and J. Butenhoff, Subchronic toxicity studies on perfluorooctanesulfonate potassium salt in cynomolgus monkeys. *Toxicol. Sci.* 68, 249 (2002).
23. K.-W. Cao, H. Huang, F.-M. Li, H.-C. Yao, J. Bai, P. Chen, P.-J. Jin, Z.-W. Deng, J.-H. Zeng, and Y. Chen, Co nanoparticles supported on three-dimensionally N-doped holey graphene aerogels for electrocatalytic oxygen reduction. *J. Colloid Interface Sci.* 559, 143 (2020).
24. B. Xiong, Y. Zhou, Y. Zhao, J. Wang, X. Chen, R. O'Hayre, and Z. Shao, The use of nitrogen-doped graphene supporting Pt nanoparticles as a catalyst for methanol electrocatalytic oxidation. *Carbon* 52, 181 (2013).
25. J. Borowiec, R. Wang, L. Zhu, and J. Zhang, Synthesis of nitrogen-doped graphene nanosheets decorated with gold nanoparticles as an improved sensor for electrochemical determination of chloramphenicol. *Electrochim. Acta.* 99, 138 (2013).
26. C. Saengsookwaow, R. Rangkupan, O. Chailapakul, and N. Rodthongkum, Nitrogen-doped graphene-polyvinylpyrrolidone/gold nanoparticles modified electrode as a novel hydrazine. *Sens. Actuators B Chem.* 227, 524 (2016).
27. H.J. Parab, C. Jung, J.-H. Lee, and H. GyuPark, A gold nanorod-based optical DNA biosensor for the diagnosis of pathogens. *Biosens. Bioelectron.* 26, 667 (2010).
28. Z. Jia, J. Liu, and Y. Shen, Fabrication of a template-synthesized gold nanorod-modified electrode for the detection of dopamine in the presence of ascorbic acid. *Electrochem. Commun.* 9, 2739 (2007).
29. M. Alagiri, P. Rameshkumar, and A. Pandikumar, Gold nanorod-based electrochemical sensing of small biomolecules: a review. *Microchim. Acta* 184, 3069 (2017).
30. J. Zheng, X. Cheng, H. Zhang, X. Bai, R. Ai, L. Shao, and J. Wang, Gold nanorods: the most versatile plasmonic nanoparticle. *Chem. Rev.* 121, 13342 (2021).
31. T.K. Sau and C.J. Murphy, Seeded high yield synthesis of short Au nanorods in aqueous solution. *Langmuir* 20, 6414 (2004).
32. P. Pang, Z. Yang, S. Xiao, J. Xie, Y. Zhang, and Y. Gao, Non-enzymatic amperometric determination of hydrogen peroxide by graphene and gold nanorods nanocomposite modified electrode. *J. Electroanal. Chem.* 727, 27 (2014).
33. X. Han, X. Fang, A. Shi, J. Wang, and Y. Zhang, An electrochemical DNA biosensor based on gold nanorods decorated graphene oxide sheets for sensing platform. *Anal. Biochem.* 443, 117 (2013).
34. A.R. Marlinda, S. Sagadevana, N. Yusoff, A. Pandikumar, N.M. Huang, O. Akbarzadeh, and M.R. Johan, Gold nanorods-coated

reduced graphene oxide as a modified electrode for the electrochemical sensory detection of NADH. *J. Alloys Compd.* 847, 156552 (2020).
35. W.S. Hummer and R.E. Offeman, Preparation of graphitic oxide. *J. Am. Chem. Soc.* 80, 1339 (1958).
36. L. Sun, L. Wang, C. Tian, T. Tan, Y. Xie, K. Shi, M. Li, and H. Fu, Nitrogen-doped graphene with high nitrogen level via a one-step hydrothermal reaction of graphene oxide with urea for superior capacitive energy storage. *RSC Adv.* 2, 4498 (2012).
37. B. Nikoobakht and M.A. El-Sayed, Preparation and growth mechanism of gold nanorods (NRs) using seed-mediated growth method. *Chem. Mater.* 15, 1957 (2003).
38. X. Xu, Y. Zhou, J. Lu, X. Tian, H. Zhu, and J. Liu, Single-step synthesis of PtRu/N-doped graphene for methanol electrocatalytic oxidation. *Electrochim. Acta.* 120, 439 (2014).
39. H. Xu, X. Liu, R. Wang, S. Gao, F. Hou, K. Liang, and S. Luo, A yellow-emitting carbon quantum dot-based fluorescent logic gate for the continuous detection of Au^{3+} and biothiols. *Chem. Commun.* 57, 11549 (2021).
40. B. Xiong, Y.K. Zhou, R. O'Hayre, and Z.P. Shao, Facile single-step ammonia heat-treatment and quenching process for the synthesis of improved Pt/N-graphene catalysts. *Appl. Surf. Sci.* 266, 433 (2013).
41. T. Kamata, D. Kato, S. Hirono, and O. Niwa, Structure and electrochemical performance of nitrogen-doped carbon film formed by electron cyclotron resonance sputtering. *Anal. Chem.* 85, 9845 (2013).
42. D.H. Guo, R. Shibuya, C. Akiba, S. Saji, T. Kondo, and J. Nakamura, Active sites of nitrogen-doped carbon materials for oxygen reduction reaction clarified using model catalysts. *Science* 351, 361 (2016).
43. H. Hibino, H. Kageshima, M. Kotsugi, F. Maeda, F.-Z. Guo, and Y. Watanabe, Dependence of electronic properties of epitaxial few-layer graphene on the number of layers investigated by photoelectron emission microscopy. *Phys. Rev. B* 79, 125437 (2009).
44. F. Li, C. Tang, S. Liu, and G. Ma, Development of an electrochemical ascorbic acid sensor based on the incorporation of a ferricyanide mediator with a polyelectrolyte-calcium carbonate microsphere. *Electrochim. Acta.* 55, 838 (2010).
45. G.P. Keeley, A. O'Neill, N. McEvoy, N. Peltekis, J.N. Colemanac, and G.S. Duesberg, Electrochemical ascorbic acid sensor based on DMF-exfoliated graphene. *J Mater. Chem.* 20, 7864 (2010).
46. S. Pakapongpan, J.P. Mensing, D. Phokharatkul, T. Lomas, and A. Tuantranont, Highly selective electrochemical sensor for ascorbic acid based on a novel hybrid graphene-copper phthalocyanine-polyaniline nanocomposites. *Electrochim. Acta.* 133, 294 (2014).
47. T.R. Das, S.K. Jena, R. Madhuri, and P.K. Sharma, Polymeric iron oxide-graphene nanocomposite as a trace level sensor of vitamin C. *Appl. Surf. Sci.* 449, 304 (2018).
48. Y. Hei, X. Li, X. Zhou, J. Liu, M. Hassan, S. Zhang, Y. Yang, X. Bo, H.-L. Wang, and M. Zhou, Cost-effective synthesis of three-dimensional nitrogen-doped nanostructured carbons with hierarchical architectures from the biomass of sea-tangle for the amperometric determination of ascorbic acid. *Anal. Chim. Acta* 1029, 15 (2018).
49. Y. Haldorai, S.R. Choe, Y.S. Huh, and Y.-K. Han, A composite consisting of microporous carbon and cobalt(III) oxide and prepared from zeolitic imidazolate framework-67 for voltammetric determination of ascorbic acid. *Microchim. Acta* 185, 116 (2018).
50. J. Scremin, E.C.M. Barbosa, C.A.R. Salamanca-Neto, P.H.C. Camargo, and E.R. Sartori, Amperometric determination of ascorbic acid with a glassy carbon electrode modified with TiO_2-gold nanoparticles integrated into carbon nanotubes. *Microchim. Acta* 185, 251 (2018).
51. K.P. Aryal, and H.K. Jeong, Electrochemical detection of ascorbic acid with chemically functionalized carbon nanofiber/β-cyclodextrin composite. *Chem. Phys. Lett.* 757, 137881 (2020).
52. Y. Jiang, X. Xiao, C. Li, Y. Luo, S. Chen, J. Shi, K. Han, and H. Gu, Facile ratiometric electrochemical sensor for in vivo/online repetitive measurements of cerebral ascorbic acid in brain microdiaysate. *Anal. Chem.* 92, 3981 (2020).

Authors and Affiliations

Shiyi Yang[1] · Yudan Cheng[1] · Deyi Cheng[1] · Yifeng Wang[1] · Hui Xu[1,4] · Mei Li[2] · Tingting Jiang[3] · Hua Wang[4,5]

✉ Hui Xu
xuhui@zjhzu.edu.cn

✉ Hua Wang
Wanghua@zjhu.edu.cn

[1] Huzhou Key Laboratory of Green Energy Materials and Battery Cascade Utilization, Department of Materials Engineering, School of Intelligent Manufacturing, Huzhou College, Huzhou 313000, People's Republic of China

[2] Department of Life and Health Sciences, Huzhou College, Huzhou 313000, People's Republic of China

[3] College of Life Sciences, Ludong University, Yantai 264025, People's Republic of China

[4] Huzhou Key Laboratory of Medical and Environmental Applications Technologies, School of Life Sciences, Huzhou University, Zhejiang 313000, People's Republic of China

[5] School of Chemistry and Chemical Engineering, Harbin Institute of Technology, Harbin 150090, Heilongjiang, People's Republic of China